IEEE Access
Multidisciplinary | Rapid Review | Open Access Journal

Received April 20, 2022, accepted May 9, 2022, date of publication May 16, 2022, date of current version May 27, 2022.

Digital Object Identifier 10.1109/ACCESS.2022.3175458

An Enhanced Photonic-Assisted Sampling Approach for Spectrum-Sparse Signal by Compressed Sensing

FANGXING LYU[1,2], FEI LI[1,2], XIN FANG[3], NAN ZHANG[1,2], AND XUEYING MA[1,2]

[1]School of Electronic Engineering, Xi'an Shiyou University, Xi'an 710065, China
[2]Shaanxi Key Laboratory of Measurement and Control Technology for Oil and Gas Wells, Xi'an 710065, China
[3]School of Computing, Xi'an Shiyou University, Xi'an 710065, China

Corresponding authors: Fei Li (lif@xsyu.edu.cn) and Xin Fang (fangxin_200610_@126.com)

This work was supported in part by the National Natural Science Foundation of China under Grant U20B2029, in part by the Key Research and Development Program of Shaanxi under Grant 2021KW-33 and Grant 2022KW-25, in part by the Natural Science Basic Research Plan in Shaanxi Province of China under Grant 2021JQ-590, and in part by the Scientific Research Program Funded by the Shaanxi Provincial Education Department under Grant 20JS125 and Grant 21JK0836.

ABSTRACT Spectrum-sparse signals are vital for wideband radar and wireless communication applications. A high-speed analog-to-digital converter (ADC) with the capacities of tens of gigahertz sampling rates is often required to acquire these signals. In this work, an enhanced photonic-assisted sampling approach with the combination of the photonic-assisted time-interleaved ADC and compressed sensing techniques is presented, which enables the measured signal to be reconstructed through very few samples by utilizing the sparsity of the spectrum-sparse signal. An ultrahigh spectral resolution Fourier dictionary was introduced to suppress the spectrum leakage and obtain the actual sparse expression of the spectrum-sparse signals. Moreover, a layered tracking orthogonal matching pursuit signal recovery algorithm was employed to reduce computational complexity and enhance processing speed. The performance of the proposed approach has been investigated via simulations and laboratory experiments by varying the applied spectrum-sparse signals over 100 times. The experimental results demonstrate that the proposed method can capture the blind-frequency spectrum-sparse signal at an equivalent sampling rate of 1 GS/s by utilizing four parallel ADCs with a sampling rate of 50 MS/s. It is proven that the proposed approach achieves ∼5 times higher equivalent sampling rate than that of the conventional PTIADC at the same sampling rate. This work provides a valuable method for acquiring spectrum sparse signals in practical applications.

INDEX TERMS Photonics-assisted ADC, compressed sensing, time-interleaved, signal recovery algorithm.

I. INTRODUCTION

Spectrum-sparse signals are crucial for many modern applications, including multi-frequency signals detection, wideband radar, wireless communication, advanced instrumentation, etc. [1], [2]. In these applications, the frequency component of these signals may be sparsely spread over a broad spectrum, and there is little prior knowledge of their frequencies. When the signal contains high-frequency components, a high-speed analog-to-digital converter (ADC) is required to realize the acquisition with the traditional Nyquist-Shannon sampling theory [3], [4]. However, it is challenging for a single ADC to achieve several tens of gigahertz sampling rates due to the inherent bandwidth bottleneck associated with electronic techniques [5], [6].

Time-interleaved ADC architecture is a well-known sampling method to overcome the bottleneck of high-speed ADCs [7]–[9]. Different sampling clocks have the same sampling rates and equally-spaced phases in this system. All outputs of multiple ADCs are recombined at the combiner to obtain a digital result, whose equivalent sampling rate is increased by a factor of M (M is the number of parallel ADCs). It should be noted that timing jitter and clock skew would be introduced by the electronically sampling clocks and environmental variations. To improve clock skew and timing jitter, a photonic-assisted time-interleaved ADC (PTIADC) scheme is proposed [9], [10]. In the PTIADC system, optically stable clocks work as sampling clocks, and an array of electronic

The associate editor coordinating the review of this manuscript and approving it for publication was Jinming Wen.

ADCs electronically quantizes the measured analog signal. Since the time jitter of optically sampling clocks is orders of magnitude better than that of electronic ones, and the phase of optically sampling clocks can be conveniently adjusted by utilizing the variable optical delay lines (VODLs), the PTIADC method enables better performance of sampling the measured analog signal [11], [12].

The emergence of compressed sensing (CS) technology provides a promising solution to improve the performance of the photonic-assisted ADC scheme. CS theory points out that if the signal itself or in a transform domain is sparse, the measured signal can be reconstructed through much fewer projections by utilizing the signal recovery algorithm [13]–[15]. The idea of CS is that the spectral information of these sparse signals is much less than their bandwidth, and few projections carry all the useful information of the original signal [16]–[18]. In 2011, Nicholsa *et al.* proposed a compressively sampled photonic link to sample 20 GHz sparse signals, which employs a 40 GHz Mach-Zehnder modulator(MZM), a Pseudo-Random Binary Sequence (PRBS) at a Nyquist rate of 40 GHz for random modulation, and with a 4 GS/s, 8-bit electrical digitizer on the output [19]. In 2012, Liang *et al.* demonstrated a photonic-assisted 8-channel CS system for Radio Frequency (RF) signal acquisition, which adopts a PRBS to generate a random measurement matrix to compress RF spectrum, and an MZM to realize multi-channel signal mixing [20]. In 2017, Guo *et al.* implemented a photonics-assisted CS system for wideband spectrum sensing. This four-channel CS system enables the acquisition of multi-tone signals with frequencies up to 5 GHz by using 120-MHz ADCs, PRBS, and intensity modulators [21]. These photonics-assisted CS schemes enable the perfect reconstruction of the spectrum-sparse signal. However, the measured signal must be mixed with PRBS at or above its Nyquist rate, which may be a challenge in these applications with ultrahigh bandwidth. Several schemes have been reported to overcome this challenge based on the approaches of optical mixing and photonic time-stretch [22]–[24]. In 2022, Yang *et al.* demonstrated a broadband signal acquisition with an ultrahigh sampling compression ratio based on continuous-time photonic time stretch and CS. The continuous-time photonic time-stretch stage can slow down the input signal and provide an unlimited sampling time aperture. Thus, the rate of PRBS can be significantly reduced [24]. However, the implementation of such a photonic time stretch module may significantly raise the system's complexity and cost.

In this work, a CS-enhanced PTIADC scheme is proposed. Unlike other PTIADC methods, the phase differences between sampling clocks are unequal-interval and randomly selected. Furthermore, an ultrahigh spectral resolution Fourier dictionary is introduced to suppress the spectrum leakage and obtain the actual sparse expression of spectrum-sparse signals in the frequency domain. In addition, a layered tracking orthogonal matching pursuit (OMP) signal recovery algorithm is advanced to reduce computational complexity. The advantage of the proposed method is a higher effective sampling rate by utilizing CS technology to reconstruct the original signal without the requirement of PRBS and the need to change the overall structure of the PTIADC system. Experimental results show that the proposed method achieves a 1 GS/s equivalent sampling rate by employing four sub-ADCs with sampling rates of 50MS/s, which is ∼5 times higher than the conventional PTIADC. These results are promising in the acquisition of spectrum-sparse signals.

II. SYSTEM CONFIGURATION AND THEORETICAL ANALYSIS

A. SAMPLING ARCHITECTURE

An illustrative scheme of the proposed CS-enhanced PTIADC sampling method is shown in Fig. 2, which comprises four parallel sampling channels (sub-ADC$_1$, sub-ADC$_2$, sub-ADC$_3$, and sub-ADC$_4$) and an optical clock module (clk$_1$, clk$_2$, clk$_3$, and clk$_4$). First, the measured spectrum sparse analog signal $E(t)$ is concurrently sampled by four parallel ADCs clocked at the same low sampling rates with the given phase differences to obtain four sampling sequences $\mathbf{E_1}$, $\mathbf{E_2}$, $\mathbf{E_3}$, and $\mathbf{E_4}$. Then these samples are re-sequenced into a set of sampling sequences $\mathbf{Y}$ (namely observation signal $\mathbf{Y}$). Subsequently, the original signal is recovered from the observation signal $\mathbf{Y}$ by utilizing the signal recovery algorithm of CS technology.

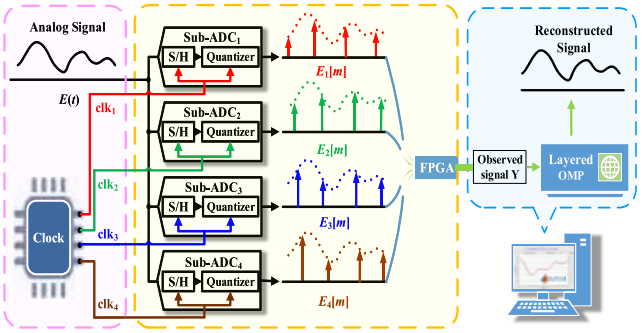

FIGURE 1. Scheme of the proposed CS-enhanced PTIADC sampling method.

Set the sampling duration of the measured signal as T, and the sampling rate of four low-rate ADCs as f_s. Let the expected high sampling rate of the recovered signal be f_e, thus the equivalent sampling time interval of the recovered signal is T_e ($T_e = 1/f_e$), and T_e has the following relationship with T

$$T_e = \frac{T}{N}, \tag{1}$$

where N is the number of samples of the expected high sampling rate recovery signal.

Let $\mathbf{E}$ denotes the samples of the measured signal quantized at the equivalent sampling rate, which can be expressed as

$$E[m] = E(mT_e), \quad 1 \le m \le N. \tag{2}$$

The sampling sequences $\mathbf{E_1}$, $\mathbf{E_2}$, $\mathbf{E_3}$, and $\mathbf{E_4}$ are obtained by four low-rate ADCs samples with the given phase differences,

which can be expressed as

$$\begin{cases} E_1[m] = E(mT_s), & 1 \le m \le M_1 \\ E_2[m] = E(mT_s + \tau_{21}), & 1 \le m \le M_2 \\ E_3[m] = E(mT_s + \tau_{31}), & 1 \le m \le M_3 \\ E_4[m] = E(mT_s + \tau_{41}), & 1 \le m \le M_4, \end{cases} \tag{3}$$

where M_1, M_2, M_3, and M_4 are the numbers of samples obtained from sub-ADC$_1$, sub-ADC$_2$, sub-ADC$_3$, and sub-ADC$_4$, respectively. τ_{21}, τ_{31}, and τ_{41} are the time differences with the first sampler, respectively. The proposed sampling method obtains M ($M = M_1 + M_2 + M_3 + M_4$) non-uniform sparse samples. Therefore, the sampling duration of the measured signal T meets

$$T = N/f_e \approx M/(4f_s) \tag{4}$$

The observation signal $\mathbf{Y}$ in the sampling duration of T can be expressed as $Y = [\mathbf{E_1}^{\mathrm{T}}, \mathbf{E_2}^{\mathrm{T}}, \mathbf{E_3}^{\mathrm{T}}, \mathbf{E_4}^{\mathrm{T}}]^{\mathrm{T}}$.

According to the CS theory, if the signal itself or in a transform domain ($\mathbf{\Psi}$ is the sparse basis matrix) is sparse, the high-dimensional signal $\mathbf{E}$ can be projected onto a low-dimensional space by constructing an eligible observation matrix $\mathbf{\Phi}$ to obtain the low-dimensional observation signal $\mathbf{Y}$, and then the signal recovery algorithm can be used to reconstruct the measured signal precisely. Therefore, the critical technology of applying CS theory in the proposed PTIADC sampling method involves the following three key technologies: the construction of sparse basis matrix $\mathbf{\Psi}$, the construction of observation matrix $\mathbf{\Phi}$,and the design of signal recovery algorithm, which is described as follows.

B. CONSTRUCTION OF ANTI-SPECTRAL LEAKAGE FOURIER DICTIONARY

Mathematically, the spectrum-sparse signal $\mathbf{E}$ can be sparsely represented in its Fourier transform domain, i.e.

$$\mathbf{E} = \mathbf{\Psi} \cdot \mathbf{X}, \tag{5}$$

where $\mathbf{\Psi}$ is the Fourier dictionary, $\mathbf{X}$ is the sparse coefficient of $\mathbf{Y}$ in $\mathbf{\Psi}$. Set a column of the matrix as an atom of the dictionary. The spectral resolution of the dictionary to the spectrum depends on the number of atoms. The number of atoms in the traditional Fourier dictionary is the number of samples N. The traditional Fourier dictionary $\mathbf{\Psi_1}$ can be expressed as

$$\mathbf{\Psi_1} = \frac{1}{\sqrt{N}} \begin{bmatrix} 1 & 1 & \cdots & 1 \\ 1 & e^{j2\pi/N} & \cdots & e^{j2\pi\times(N-1)/N} \\ 1 & e^{j2\pi\times2/N} & \cdots & e^{j2\pi\times2\times(N-1)/N} \\ \vdots & \vdots & \ddots & \vdots \\ 1 & e^{j2\pi\times(N-1)/N} & \cdots & e^{j2\pi\times(N-1)\times(N-1)/N} \end{bmatrix}. \tag{6}$$

In Eq. (6), the traditional Fourier dictionary is composed of N atoms with different frequency characteristics, each atom represents a frequency characteristic $(0, f_e/N, \ldots, (N\text{-}1)f_e/N)$, and the spectral resolution is f_e/N.

As N is finite, some energy of the signal may leak out of the original signal spectrum into other frequencies, which shows up as a series of "lobes" with the phenomenon of "spectral leakage". At this time, the measured original signal characteristics need to be characterized by more atoms of the dictionary. Thus, to suppress the spectral leakage, an ultrahigh-frequency resolution fine Fourier dictionary is addressed, which can be expressed as

$$\mathbf{\Psi}_2 = \frac{1}{N} \begin{bmatrix} 1 & 1 & \cdots & 1 \\ 1 & e^{j2\pi/(pN)} & \cdots & e^{j2\pi\times(pN-1)/(pN)} \\ 1 & e^{j2\pi\times2/(pN)} & \cdots & e^{j2\pi\times2\times(pN-1)/(pN)} \\ \vdots & \vdots & \ddots & \vdots \\ 1 & e^{j2\pi\times(N-1)/(pN)} & \cdots & e^{j2\pi\times(N-1)\times(pN-1)/(pN)} \end{bmatrix}, \tag{7}$$

where p is the multiple of spectral resolution coefficient. The spectral resolution of the fine dictionary $\mathbf{\Psi_2}$ is $f_e/(pN)$, and it would be closer to the actual sparse coefficient in the fine dictionary $\mathbf{\Psi_2}$ than in the traditional Fourier dictionary $\mathbf{\Psi_1}$.

C. CONSTRUCTION OF OBSERVATION MATRIX

The physical meaning of observation matrix $\mathbf{\Phi}$ indicates the way of sparse sampling. The high-dimensional signal $\mathbf{E}$ obtained at the expected high equivalent sampling rate f_e is mapped to the sparse signal $\mathbf{Y}$ from four sub-ADCs by an eligible observation matrix $\mathbf{\Phi}$, namely

$$\mathbf{Y} = \mathbf{\Phi} \cdot \mathbf{E}, \tag{8}$$

The observation matrix $\mathbf{\Phi}$ can be constructed based on the detailed physical observation process in the proposed method. According to the Whittaker–Shannon interpolation theory, $E(t)$ can be represented by the sampling value $E(nT_e)$ ($n = 1, 2, \ldots, N$) under the condition that the samples are quantized at the expected high equivalent sampling rate f_e, i.e.

$$E(t) \approx \sum_{n=1}^{N} E(nT_e) \cdot \sin c\left(\frac{t}{T_e} - n\right). \tag{9}$$

Take Eq. (9) into Eq. (3), then Eq. (3) can be rewritten as

$$\begin{cases} E_1[m] \approx \sum_{n=1}^{N} E(nT_e) \cdot \sin c\left(\frac{mT_s}{T_e} - n\right), & 1 \le m \le M_1 \\ E_2[m] \approx \sum_{n=1}^{N} E(nT_e) \cdot \sin c\left(\frac{mT_s + \tau_{21}}{T_e} - n\right), & 1 \le m \le M_2 \\ E_3[m] \approx \sum_{n=1}^{N} E(nT_e) \cdot \sin c\left(\frac{mT_s + \tau_{31}}{T_e} - n\right), & 1 \le m \le M_3 \\ E_4[m] \approx \sum_{n=1}^{N} E(nT_e) \cdot \sin c\left(\frac{mT_s + \tau_{31}}{T_e} - n\right), & 1 \le m \le M_4 \end{cases} \tag{10}$$

From Eq. (10), it can be seen that high-dimensional signal $\mathbf{E}$ at a high sampling rate can be mapped to the low-dimensional sampling sequences $\mathbf{E_1}$, $\mathbf{E_2}$, $\mathbf{E_3}$, and $\mathbf{E_4}$ at the low-rate samplers through a certain mapping relationship, namely

$$\begin{cases} \mathbf{E_1} = \boldsymbol{\phi}\mathbf{E} \\ \mathbf{E}_2 = \boldsymbol{\varphi}\mathbf{E} \\ \mathbf{E}_3 = \boldsymbol{\gamma}\mathbf{E} \\ \mathbf{E}_4 = \boldsymbol{\eta}\mathbf{E}, \end{cases} \tag{11}$$

where ϕ, φ, γ and $\boldsymbol{\eta}$ are the matrices motivated by four low-rate sub-ADCs respectively, which can be expressed as

$$\begin{cases} \phi(m,n) = \sin c\left(\dfrac{mT_s}{T_e} - n\right), \quad 1 \le m \le M_1, 1 \le n \le N \\ \varphi(m,n) = \sin c\left(\dfrac{mT_s + \tau_{21}}{T_e} - n\right), \\ \qquad\qquad 1 \le m \le M_2, 1 \le n \le N \\ \gamma(m,n) = \sin c\left(\dfrac{mT_s + \tau_{31}}{T_e} - n\right), \\ \qquad\qquad 1 \le m \le M_3, 1 \le n \le N \\ \eta(m,n) = \sin c\left(\dfrac{mT_s + \tau_{41}}{T_e} - n\right), \\ \qquad\qquad 1 \le m \le M_4, 1 \le n \le N \end{cases} \tag{12}$$

From the perspective of CS theory, the essence of the observation matrix $\boldsymbol{\Phi}$ is mapping the signal from high-dimensional space to low-dimensional space to get sparse observation signal $\mathbf{Y}$. Thus, the observation matrix $\boldsymbol{\Phi}$ is the mathematical expression of the mapping relationship, which can be expressed as

$$\boldsymbol{\Phi} = [\boldsymbol{\phi}^{\mathrm{T}}, \boldsymbol{\varphi}^{\mathrm{T}}, \boldsymbol{\gamma}^{\mathrm{T}}, \boldsymbol{\eta}^{\mathrm{T}}]^{\mathrm{T}}. \tag{13}$$

Some studies have proved that when the correlation coefficient between the observation matrix $\boldsymbol{\Phi}$ and the sparse dictionary $\boldsymbol{\Psi}$ is less than 0.2, the observation matrix $\boldsymbol{\Phi}$ is eligible [25]–[27]. The correlation coefficient between $\boldsymbol{\Phi}$ and $\boldsymbol{\Psi_2}$ can be calculated by

$$\boldsymbol{\mu}(\boldsymbol{\Phi}, \boldsymbol{\Psi}_2) = \max \left|\langle \boldsymbol{\varphi}_i, \boldsymbol{\psi}_{2_k} \rangle\right|, \tag{14}$$

where $\boldsymbol{\varphi}_i$ and $\boldsymbol{\psi}_{2k}$ are any atom of $\boldsymbol{\Phi}$ and $\boldsymbol{\Psi_2}$, respectively. The smaller the correlation coefficient is, the better the observation matrix performance is, and the observation signal Y carries more information of the original signal E. To preserve the integrity of the original data information, the number of sparse samples should meet $M \ge 2K\ln(N/K)$, where K is the sparsity of the original signal $\mathbf{E}$ [26]. By substituting different N and K into this equation, the requirements of M can be calculated. The larger the K value is, the larger M is required.

To ensure less correlation of the observation matrix $\boldsymbol{\Phi}$ and the sparse dictionary $\boldsymbol{\Psi}$, the phase difference is randomly selected. In this work, τ_{21}, τ_{31}, and τ_{41} are randomly set as $3T_e$, $11T_e$, and $16T_e$, respectively. The results of the correlation coefficient are shown in Tab. 1. As shown in Tab.I, the correlation coefficient between $\boldsymbol{\Phi}$ and $\boldsymbol{\Psi_2}$ under different spectral resolution coefficients p is small than 0.1, which shows that the constructed observation matrix is eligible.

TABLE 1. Calculation results of correlation coefficient.

N	p=1	p=10	p=20	p=30
300	0.058	0.099	0.099	0.099
500	0.045	0.077	0.077	0.077
1000	0.032	0.055	0.055	0.055
2000	0.022	0.039	0.039	0.039

D. DESIGN OF LAYERED TRACKING ORTHOGONAL MATCHING PURSUIT ALGORITHM

Taking Eq. (5) into Eq. (8), the relationship between the non-uniform samples $\mathbf{Y}$ of size M and the uniform equivalent samples $\mathbf{E}$ of size N can be furthermore expressed by the following matrix-vector representation

$$\mathbf{Y} = \boldsymbol{\Phi} \cdot \mathbf{E} = \boldsymbol{\Phi} \cdot \boldsymbol{\Psi}_2 \cdot \mathbf{X}_2 = \mathbf{A}_2 \cdot \mathbf{X}_2, \tag{15}$$

where $\mathbf{A}_2 = \boldsymbol{\Phi} \cdot \boldsymbol{\Psi}_2$ is the sensing matrix. As shown in Eq. (15), the dimension of $\mathbf{Y}$ is much lower than that of $\mathbf{E}(M < N)$. Therefore, reconstructing $\mathbf{E}$ from $\mathbf{Y}$ is an ill-posed problem, and there may be many possible solutions to Eq. (15). To recover $\mathbf{E}$, a signal recovery algorithm is required. The purpose of the signal recovery algorithm is to find the sparsest solution of $\mathbf{X_2}$ that contains the minimum number of nonzero sparse coefficients in the following formulation, i.e.

$$\min \|\mathbf{X}_2\|_0 \quad \text{s.t. } \|\mathbf{r}\|_2 = \|\mathbf{A}_2 \cdot \mathbf{X}_2 - \mathbf{E}\|_2 < \varepsilon, \tag{16}$$

where $\mathbf{r}$ is the signal residual, $\|\cdot\|$ is the Euclidean norm, and ε is the threshold of $\mathbf{r}$.

In general, the signal recovery algorithms are divided into two categories: convex relaxation algorithm and greedy algorithm. Compared with the convex relaxation algorithm, the greedy method is more efficient and easier to implement, thus it has been widely used in engineering practice. One of the fundamental greedy pursuit techniques is Orthogonal Matching Pursuit (OMP) [28], [29], which has some variants such as the regularized OMP (ROMP)[30], Stagewise OMP (StOMP) [31], Subspace Pursuit (SP) [32], Compressed Sampling Matching Pursuit (CoSaMP) [33], and batch-OMP [34]. They are the iterative algorithms that try to find the best approximation of $\mathbf{X_2}$ after some iterations. However, when the atoms of the fine dictionary $\boldsymbol{\Psi_2}$ increase sharply with spectral resolution coefficients p, the computational complexity of these algorithms also increases rapidly. In 2021, a binary matching pursuit (BMP) method was proposed to recover the sparse binary signal [35]. However, the BMP method is only suitable for sparse binary signals.

In this work, a layered tracking OMP algorithm is proposed. The traditional Fourier dictionary $\boldsymbol{\Psi_1}$ is used as the index dictionary, $\boldsymbol{\Psi_1}$ is a subset of $\boldsymbol{\Psi_2}$, and $\boldsymbol{\Psi_1}$ has far fewer

atoms than $\mathbf{\Psi_2}$. Eq. (15) can be rewritten as

$$\begin{cases} \mathbf{Y} = \mathbf{\Phi} \cdot \mathbf{E} = \mathbf{\Phi} \cdot \mathbf{\Psi 1} \cdot \mathbf{X_1} = \mathbf{A_1} \cdot \mathbf{X_1} & (1) \\ \mathbf{Y} = \mathbf{\Phi} \cdot \mathbf{E} = \mathbf{\Phi} \cdot \mathbf{\Psi_2} \cdot \mathbf{X_2} = \mathbf{A}_2 \cdot \mathbf{X_2} & (2), \end{cases} \tag{17}$$

where $\mathbf{A_1}$ and $\mathbf{A_2}$ are the high-frequency resolution and low-frequency resolution sensing matrices, respectively. In the process of signal reconstruction, the approximate spectrum range of the signal is firstly determined through the index dictionary $\mathbf{\Psi_1}$, and then a corresponding partial interval of the fine dictionary $\mathbf{\Psi_2}$ is used to make the further sparse expression in the spectrum range. In this way, the sparse expression of the high-frequency resolution of the signal is realized, and the total number of atoms required to project the signal is significantly reduced. The flowchart of the proposed layered tracking OMP algorithm is shown in Fig.2, which can be illustrated as follows.

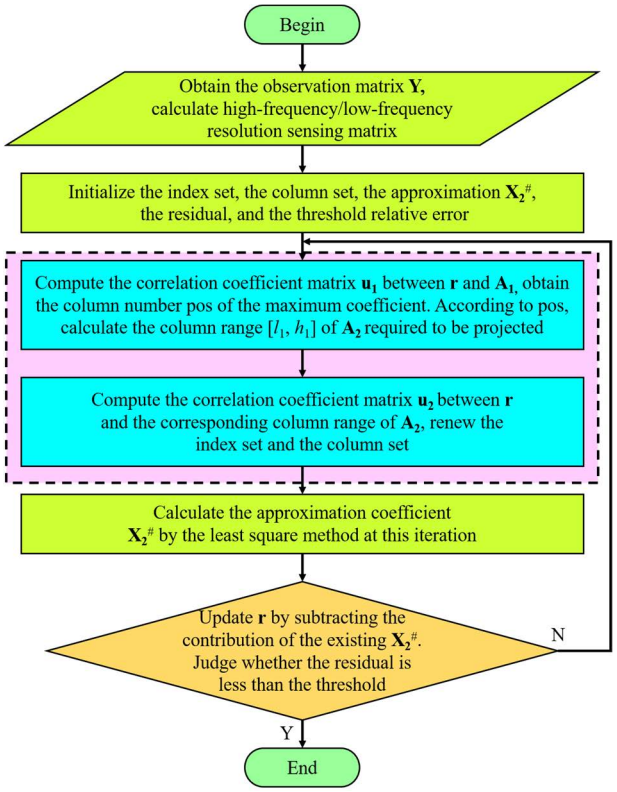

FIGURE 2. The flowchart of the layered tracking OMP algorithm.

Definition: $\mathbf{u_1}$ denotes the correlation coefficient matrix with the low spectral resolution, while $\mathbf{u_2}$ denotes the correlation coefficient matrix with high spectral resolution. $\mathbf{r}$ denotes the residual vector, i denotes the number of iterations, $\mathbf{s_i}$ denotes the index set at the ith iteration, $\mathbf{B}_\mathrm{i}$ denotes the column set of sensing matrix $\mathbf{A_2}$ corresponding to the index, λ denotes the foot mark value of the column vector of $\mathbf{A_2}$ corresponding to the largest correlation coefficient selected.

Input: The sensing matrix with low spectral resolution $\mathbf{A_1}$, The sensing matrix with high spectral resolution $\mathbf{A_2}$, the observation matrix $\mathbf{Y}$ from four sub-ADCs, and the relative error ε.

Output: The approximation $\mathbf{X_2}^{\#}$ of $\mathbf{X_2}$.

Step 1: Initialize the index set $\mathbf{s_0}$, the column set $\mathbf{B_0}$ and the approximation $\mathbf{X_2}^{\#}$ to an empty set, and the residual $\mathbf{r}$ to $\mathbf{Y}$. Set a pre-determined threshold relative error $\varepsilon = 4{*}10^{-2}$, the number of iterations $i = 1$.

Step 2: Compute every column of the correlation coefficient matrix $\mathbf{u_1}$ with the low spectral resolution, which can be expressed as

$$\mathbf{u_1} = \left\{ u_{1_\mathrm{j}} \left| u_{1_\mathrm{j}} = \frac{\langle \mathbf{A}_{1_\mathrm{j}}{}^{\mathbf{T}}, \mathbf{r} \rangle}{\left\| \mathbf{A}_{1_\mathrm{j}}{}^{\mathbf{T}} \right\| \|\mathbf{r}\|} \right. | j \in [l_1, h_1] \right\}. \tag{18}$$

Find the maximum coefficient column number pos of $\mathbf{A_1}$ corresponding to $\mathbf{u_1}$, and calculate the column range $[l_1, h_1]$ of $\mathbf{A_2}$ required to be projected according to pos:

$$\begin{cases} l_1 = \dfrac{pN}{q}(pos - 1) \\ h_1 = \dfrac{pN}{q}(pos + 1). \end{cases} \tag{19}$$

Step 3: Compute every column of the correlation coefficient matrix $\mathbf{u_2}$ corresponding to the column range $[l_1, h_1]$ of $\mathbf{A_2}$, i.e.

$$\mathbf{u}_2 = \left\{ u_{2_\mathrm{j}} \left| u_{2_\mathrm{j}} = \frac{\langle \mathbf{A}_{2_\mathrm{j}}{}^{\mathbf{T}}, \mathbf{r} \rangle}{\left\| \mathbf{A}_{2_\mathrm{j}}{}^{\mathbf{T}} \right\| \|\mathbf{r}\|} \right. | j \in [l_1, h_1] \right\}. \tag{20}$$

Select the largest correlation coefficient, store the corresponding foot mark to λ, and update the index set $\mathbf{s}_i$, i.e., $\mathbf{s}_i = \mathbf{s}_{i-1} \cup \{\lambda\}$. Then renew the column set $\mathbf{B}_i$ by the union of the corresponding column of sensing matrix $\mathbf{A}$, i.e. $\mathbf{B}_i = \left[\mathbf{B}_{i-1}, \mathbf{A}_{2_\lambda}\right]$, and set the corresponding column vector $\mathbf{A}_{2_\lambda}$ to 0.

Step 4: Calculate the approximation coefficient $\mathbf{X_2}^{\#}$ by the least square method at this iteration by the least square method, i.e.

$$\mathbf{X_2}^{\#} = (\mathbf{B_i}^{\mathbf{T}}\mathbf{B_i})^{-1}\mathbf{B_i}^{\mathbf{T}}\mathbf{r}. \tag{21}$$

Then update $\mathbf{r}$ by subtracting the contribution of the existing $\mathbf{X_2}^{\#}$, namely

$$\mathbf{r} = \mathbf{Y} - \mathbf{B_i}\mathbf{X_2}^{\#}. \tag{22}$$

Step 5: Repeat Steps 2–4 until the Euclidean norm of the updated residual $\mathbf{r}$ meets a pre-determined threshold ε.

At last, we can obtain the approximation $\mathbf{X_2}^{\#}$ of $\mathbf{X}$ and reconstruct the original signal through Eq. (17). In this way, the total number of projection atoms increases little, and the projection effect of the fine dictionary $\mathbf{\Psi_2}$ is achieved. Also, some parallel eigenvalue algorithms by using rank-structured matrix techniques can be used to compute the correlation coefficient matrix to accelerate our algorithms [36], [37].

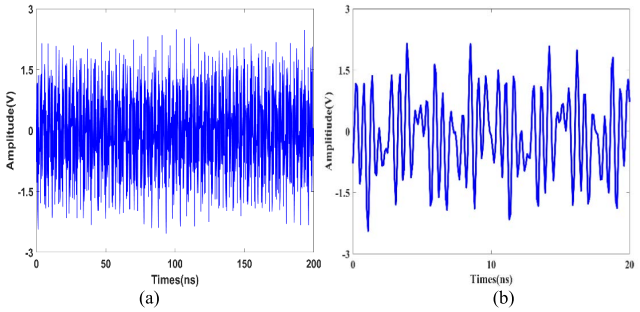

FIGURE 3. (a) Waveform of original signal. (b) Locally enlarged images.

III. NUMERICAL SIMULATION AND ANALYSIS

A. SIMULATION PARAMETER SETTING

In this simulation, the multiple spectral resolution coefficient is set as $p = 20$. The expected high equivalent sampling rate of the reconstructed signal is set as $f_e = 10$ GS/s, and the sampling duration of the measured signal is set as $T = 200$ns. Thus, the equivalent sample of the reconstructed signal is $N = 2000$. The number of frequency components of the spectrum-sparse signal is set as $j = 5$. Thus, the sparsity of the measured signal K is larger than 5, as the possible spectrum leakage. As illustrated in "Section 3", the number of sparse samples should meet $M \geq 2K \ln(N/K)$, where K is the sparsity of the measured signal. To make room for the possible increase of the sparsity K, the sparse sample M is set as 400 ($M_1 = M_2 = M_3 = M_4 = 100$), and the sampling rate of four sub-ADCs is $f_s = 500$ MS/s calculated through Eq. (4).

B. SIMULATION RESULT AND ANALYSIS

A spectrum-sparse signal is used to demonstrate the proposed CS-enhanced PTIADC scheme, which can be expressed as

$$E(t) = \sum_{i=1}^{j} E_i \cos(2\pi f_i t - p_i), \tag{23}$$

where E_i, f_i, *and* p_i represent the amplitude, frequency, and phase of each frequency component, respectively. E_1, E_2, E_3, E_4 and E_5 are randomly set as 0.91, 0.34, 0.86, 0.72 and 0.47, respectively. f_1, f_2, f_3, f_4 and f_5 are randomly set as 1.558143066 GHz, 0.185463435 GHz, 1.94794244 GHz, 0.000089598 GHz and 0.87573014GHz, respectively. p_1, p_2, p_3, p_4, and p_5 are randomly set as $\pi/12$, $37\pi/40$, $-2\pi/3$, $-\pi/30$, and $-\pi/5$, respectively. τ_{21}, τ_{31} and τ_{41} are randomly set as 0.3ns, 3.3ns, and 4.8ns, respectively. The waveform of the spectrum-sparse signal and its locally enlarged image are shown in Fig. 3.

First off, according to Eq. (4), four sampling sequences are captured and re-sequenced into the sparse observation signal $\mathbf{Y}$ by four parallel sub-Nyquist ADCs, which are shown in Fig. 4.

Moreover, the index Fourier dictionary $\mathbf{\Psi_1}$ and fine Fourier dictionary $\mathbf{\Psi_2}$ are achieved by Eq. (6) and Eq. (7). As an index Fourier dictionary, $\mathbf{\Psi_1}$ has 2000 atoms with the length of 2000 and divides f_e into 2000 frequency bands, the spectral resolution of $\mathbf{\Psi_1}$is $f_e/2000 = 5$ MHz; As a fine Fourier dictionary, $\mathbf{\Psi_2}$ has 40000 atoms with the length of 2000 and divides f_e into 40000 frequency bands, while the spectral resolution of $\mathbf{\Psi_2}$ is $f_e/40000 = 0.25$ MHz. The observation matrix $\mathbf{\Psi}$ would be constructed through Eq. (12). After that, we reconstruct the signal by the proposed layered OMP algorithm described in "Section 2", which is illustrated as follows.

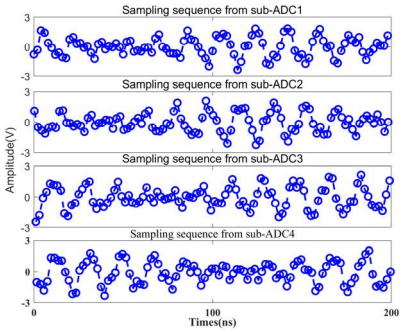

FIGURE 4. (a) Schematic diagram of photonic time-interleaving ADC. (b) Sampling clocks.

The high and low spectral resolution sensing matrices $\mathbf{A_1}$ and $\mathbf{A_2}$ are calculated by Eq. (16). In the first iteration, the projection result of the signal residual $\mathbf{r}$ in $\mathbf{A_1}$ is shown in Fig. 5 (a). As shown in Fig. 5 (a), the column with the largest projection coefficient in $\mathbf{A_1}$ is column 313. From this, it can be calculated that the corresponding column range required to be projected in $\mathbf{A_2}$is columns 6220∼6260. The projection result of the signal residual $\mathbf{r}$ in columns 6220 ∼ 6260 of $\mathbf{A_2}$ is shown in Fig. 5 (b). As shown in Fig. 5 (b), the column with the largest projection coefficient in $\mathbf{A_2}$is column 6234. Thus the best $\mathbf{\Psi_2}$ atom represented the characteristics of the original signal in the first iteration is the 6234th atom. The correlation coefficient is updated by subtracting the contribution of the selected 6234th atom in "Step 4", which is shown in Fig. 5 (c). Repeat the iteration process, and the approximation $\mathbf{X_2}^{\#}$ of $\mathbf{X_2}$ would be achieved to reconstruct the signal until the Euclidean norm of$\mathbf{r}$ is lower than the preset threshold ε (see Fig. 5 (d)).

Fig. 6 shows the reconstructed and original waveform of the spectrum-sparse signal and its locally enlarged image, respectively. As shown in Fig. 6, the time interval between two adjacent points of the reconstructed signal is 10^{-10} s, which means that the equivalent sampling rate of 10 GS/s has been achieved. The sampling rate of four parallel ADCs is 500 MS/s, which is lower than one-twentieth of the equivalent sampling rate of the reconstructed signal. Moreover, the reconstructed waveform is well coincident with the original waveform. The quality of the reconstructed signal can be evaluated by the Signal-to-noise ratio (*SNR*), which can be defined as

$$\boldsymbol{SNR} = 20 \cdot \log_{10} \frac{\|\mathbf{E}\|}{\|\mathbf{E} - \mathbf{E}'\|}, \tag{24}$$

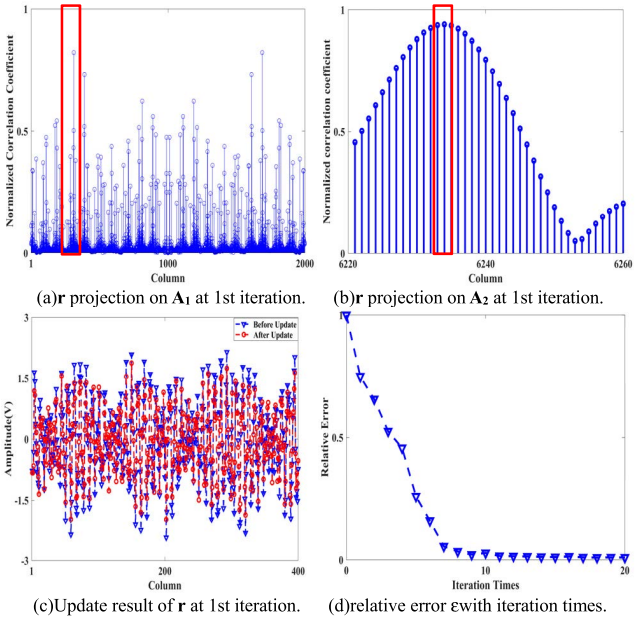

(a)**r** projection on $\mathbf{A}_1$ at 1st iteration. (b)**r** projection on $\mathbf{A}_2$ at 1st iteration.
(c)Update result of **r** at 1st iteration. (d)relative error ε with iteration times.

FIGURE 5. The recovery process of the measured signal.

where $\mathbf{E}'$ is the reconstructed signal. The *SNR* of the reconstructed signal is calculated to be 60.8 dB, which means that the original signal is well recovered. After replacing the random values of amplitude, frequency, and phase in Eq. (23) and reconstructing the corresponding signal, we can obtain that the mean of the *SNR* values over 100 times is 61.2 dB. Therefore, the feasibility of the proposed method has been demonstrated.

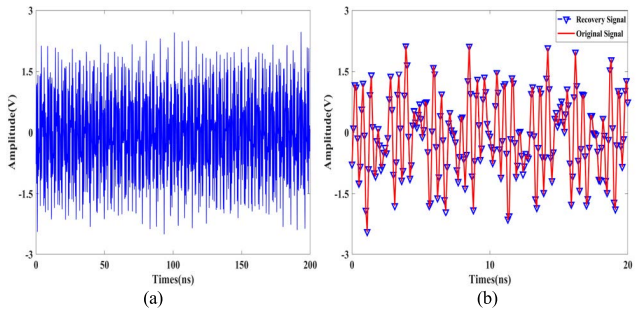

(a) (b)

FIGURE 6. (a) Waveform of recovery signal. (b) Locally enlarged images.

Moreover, the reconstructed effects for the signals composed of infinite frequency components such as square wave and triangular wave signals are investigated. The acquisition processes of these signals are similar to that of the spectrum-sparse signal. Fig.7 shows the reconstructed and original waveforms of square wave and triangular wave signals obtained by the proposed method. As shown in Fig.7, the reconstructed signals are less coincident with the original signals than in the case of spectrum-sparse signals. This is because these signals have infinite frequency components in the frequency domain and cannot be sparsely expressed by the Fourier dictionary.

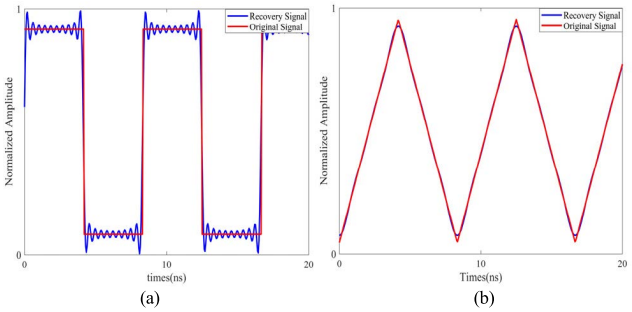

(a) (b)

FIGURE 7. (a) The recovery waveform of the square wave signal. (b) The recovery waveform of the triangular wave signal.

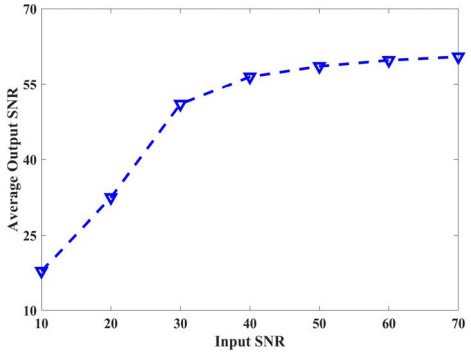

FIGURE 8. Average SNR of the recovery signal in the different noise levels.

Also, we evaluate the robustness of the proposed method by adding Gaussian white noise to the original signal. When the noise of the original signal increases from 10 to 70 dB, the mean of the SNR values under each noise condition are plotted in Fig. 8. As shown in Fig. 8, when the noise is high, we can still recover the original signal very well. This proves that the proposed sampling method has good robustness against the Gaussian noise.

IV. EXPERIMENTS AND DISCUSSIONS

A. EXPERIMENTAL SET-UP

Fig. 9 shows the experimental set-up of the proposed CS-enhanced PTIADC system, which consists of an optical clock module and an electrical acquisition module. First, the optical clock module is used to generate four sampling clock signals of low-rate ADCs with a certain phase difference. Then the measured spectrum sparse analog signal is concurrently sampled by four parallel low-rate ADCs to obtain the observation signal $\mathbf{Y}$. At last, the measured signal is recovered by utilizing the proposed layered OMP algorithm.

In our experiment, the expected high equivalent sampling rate of the reconstructed signal is $f_e = 1$ GS/s, and the sampling rates of sub-ADCs are $f_S = 50$MS/s. The sampling duration of the measured signal is $T = 2\mu$ s. The number of the reconstructed signal is $N = 2000$, while the total sampling number of sub-ADCs is $M = 400$. The time differences with the first sampler τ_{21}, τ_{31}, and τ_{41} are 1.5ns, 5.5ns, and 8.0ns, respectively. In the electrical sampling

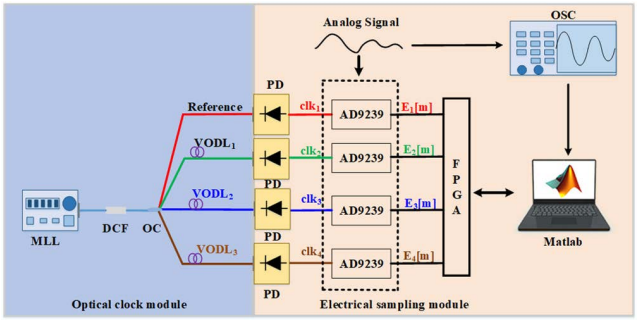

FIGURE 9. Experimental set-up of the proposed sampling system.

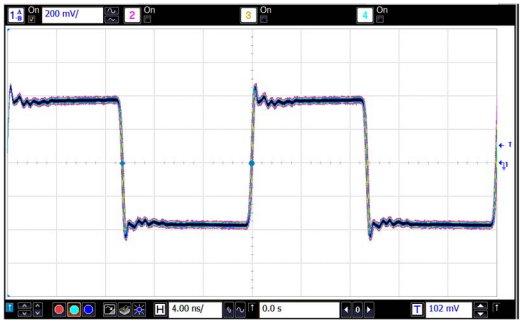

FIGURE 10. Sampling clocks picture with the eye diagram.

module, the measured analog signal is commonly sampled by four parallel low-speed sub-ADCs (AD9239s from Analog Devices Inc.) clocked at 50MS/s, which is far lower than the expected high equivalent sampling rate. The maximum sampling rate of ADC (AD9239) can reach 170MS/s, and the full-power Bandwidth (FPBW) is 780MHz. After the acquisition, these samples are re-sequenced into a group of low-speed sampling sequences, which act as the sparse signal Y. Then, the measured signal would be reconstructed by solving the optimization problem described by Eq. (12). Simultaneously, the measured signal is also collected by a wideband oscilloscope (DSO9254A from Agilent Inc.) as the reference signal to evaluate the reconstructed signal.

B. EXPERIMENTAL RESULTS AND ANALYSIS

The optical clock module consists of a mode-locked laser (MLL) as the optical pulse source, a dispersion compensation fiber (DCF) as the dispersive medium, a 1×4 optical coupler, and three VODLs. Initially, an ultra-low-jitter pulse with a duration of ∼200fs is generated from MLL, which has extremely low noise with a repetition period of 20ns. After the optical pulse propagates into DCF, the duration of the optical pulse is stretched to nanosecond order, which can offer sufficient time for the optical-electronic devices to respond. Then the stretched optical pulse is evenly divided into four channels by a 1×4 optical coupler. To get the pre-designed phase delays, the parallel optical signals propagate via a set of VODLs. Then the parallel optical clock signals with the given phase differences would be obtained by high-speed PDs and signal conditioning circuit. However, jitter degradation inevitably exists because the optical clocks should go through optic-electronic conversion as well as electrical condition-stage before being fed into the ADCs. To evaluate the timing jitter clock, we used the same oscilloscope to monitor the clock signal in accumulation mode. Fig. 10 shows a histogram on the falling edge of the clock output. The histogram measures the statistics of the time when this edge crosses a given voltage, which is zero in this measurement. The root-mean-square (RMS) jitter or one standard deviation of the histogram was around 15.5 ps, which is acceptable for a 50M sampling clock. And then, these clock signals flow into the electrical acquisition module and act as the sampling clock signals of ADCs.

In the cause of investigating the performance of the proposed method, a multi-tone signal acted as the spectrum-sparse signal is generated by the arbitrary signal generator, which is shown in Fig. 11.

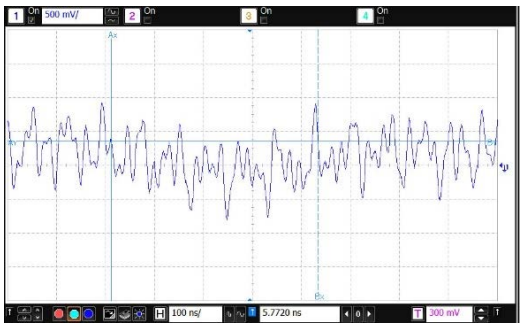

FIGURE 11. The waveform of the measured signal generated by the arbitrary signal generator.

Firstly, four sampling sequences are captured by four parallel ADCs, and the sparse observation signal $\mathbf{Y}$is obtained. What's more, the index Fourier dictionary $\mathbf{\Psi_1}$ and fine Fourier dictionary $\mathbf{\Psi_2}$ are achieved by Eq. (6) and Eq. (7). As an index Fourier dictionary, $\mathbf{\Psi_1}$ has 2000 atoms with the length of 2000 and divides f_e into 2000 frequency bands, the spectral resolution of $\mathbf{\Psi_1}$ is $f_e/2000 = 0.5$ MHz; As a fine Fourier dictionary, $\mathbf{\Psi_2}$ has 40000 atoms with the length of 2000 and divides f_e into 40000 frequency bands, while the spectral resolution of $\mathbf{\Psi_2}$ is $f_e/40000 = 25$ kHz. The observation matrix $\mathbf{\Phi}$ would be constructed by using Eq. (12). At last, the measured signal is reconstructed by the proposed layered tracking OMP algorithm and displayed in our LabVIEW-based procedure, which is shown in Fig. 12.

As shown in Fig. 12(b), the time interval between two adjacent points of the reconstructed signal is 10^{-9} s, which means that the equivalent sampling rate of 1 GS/s has been achieved. The *SNR* of the reconstructed signal is calculated to be 53.6 dB by Eq. (24), which indicates that the recovery waveform is well coincident with the reference waveform recorded by the OSC. Compared with the simulation results in "Section 3", the *SNR* of the recovery signal obtained by the proposed system is smaller. The reason is that in the actual

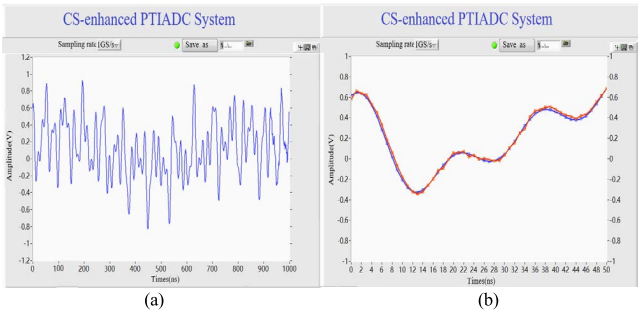

(a) (b)

FIGURE 12. **(a) Waveform of the recovery signal. (b) Locally enlarged images.**

sampling experiment, the sampling clock of four parallel ADCs has a clock jitter, and the sampling results also have deviation.

V. CONCLUSION

An enhanced photonic-assisted sampling approach based on PTIADC and CS technology is proposed and validated. The performance of the proposed method has been investigated via simulations and laboratory experiments by varying the applied spectrum-sparse signals. Simulations show that the proposed method can achieve the equivalent sampling rate of 10 GS/s by four sub-ADCs with sampling rates of 500 MS/s. By using an optical clock module, a proof-of-concept experiment was carried out to demonstrate that the spectrum-sparse signals with blind frequencies can be well reconstructed. The ratio of the equivalent sampling rate to the average sampling rate is 20, which is higher than that of the conventional PTIADC system using four ADCs clocked at the same sampling rates. These results are encouraging for the development of the high-frequency spectrum-sparse signal acquisition in practical applications. Moreover, some parallel methods to improve the practicability and speed of the signal recovery algorithm should be considered in our future work.

ACKNOWLEDGMENT

The authors would like to thank Hui Ding, Zhongying Wu, Chunyang Han, and Haichen Zhao for the helpful discussions.

REFERENCES

[1] I. Andráš, P. Dolinský, L. Michaeli, and J. Šaliga, "A Time domain reconstruction method of randomly sampled frequency sparse signal," *Measurement*, vol. 127, pp. 68–77, May 2018, doi: 10.1016/j.measurement.2018.05.065.

[2] M. B. Mashhadi, S. Gazor, N. Rahnavard, and F. Marvasti, "Feedback acquisition and reconstruction of spectrum-sparse signals by predictive level comparisons," *IEEE Signal Process. Lett.*, vol. 25, no. 4, pp. 496–500, Apr. 2018, doi: 10.1109/LSP.2018.2801836.

[3] C. L. Farrow, M. Shaw, H. Kim, P. Juhás, and S. J. L. Billinge, "The Nyquist-Shannon sampling theorem and the atomic pair distribution function," *Phys. Rev. B, Condens. Matter*, vol. 84, no. 13, pp. 4578–4586, May 2012, doi: 10.1103/PhysRevB.84.134105.

[4] P. L. Butzer, G. Schmeisser, and R. L. Stens, "Shannon's sampling theorem for bandlimited signals and their Hilbert transform, Boas-type formulae for higher order derivatives-the aliasing error involved by their extensions from bandlimited to non-bandlimited signals," *Entropy*, vol. 14, no. 11, pp. 2192–2226, Oct. 2012, doi: 10.3390/e14112192.

[5] R. H. Walden, "Analog-to-digital conversion in the early twenty-first century," in *Wiley Encyclopedia of Computer Science and Engineering*. New York, NY, USA: Wiley, Sep. 2008, pp. 1–14, doi: 10.1002/9780470050118.ecse014.

[6] A. T. Ramkaj, J. C. P. Ramos, M. J. M. Pelgrom, M. S. J. Steyaert, M. Verhelst, and F. Tavernier, "A 5-GS/s 158.6-mW 9.4-ENOB passive-sampling time-interleaved three-stage pipelined-SAR ADC with analog–digital corrections in 28-nm CMOS," *IEEE J. Solid-State Circuits*, vol. 55, no. 6, pp. 1553–1564, Jun. 2020, doi: 10.1109/JSSC.2019.2960476.

[7] E. Swindlehurst, H. Jensen, A. Petrie, Y. Song, Y.-C. Kuan, Y. Qu, M.-C. F. Chang, J.-T. Wu, and S.-H. W. Chiang, "An 8-bit 10-GHz 21-mW time-interleaved SAR ADC with grouped DAC capacitors and dual-path bootstrapped switch," *IEEE J. Solid-State Circuits*, vol. 56, no. 8, pp. 2347–2359, Aug. 2021, doi: 10.1109/JSSC.2021.3057372.

[8] X. Li, J. Wu, and C. Vogel, "A background correlation-based timing skew estimation method for time-interleaved ADCs," *IEEE Access*, vol. 9, pp. 45730–45739, 2021, doi: 10.1109/ACCESS.2021.3067355.

[9] C. Xu, S. Zheng, X. Chen, H. Chi, X. Jin, and X. Zhang, "Photonic-assisted time-interleaved ADC based on optical delay line," *J. Opt.*, vol. 18, no. 1, Jan. 2016, Art. no. 015704, doi: 10.1088/2040-8978/18/1/015704.

[10] G. Yang, W. Zou, L. Yu, K. Wu, and J. Chen, "Compensation of multi-channel mismatches in high-speed high-resolution photonic analog-to-digital converter," *Opt. Exp.*, vol. 24, no. 21, pp. 24061–24074, 2016, doi: 10.1364/oe.24.024061.

[11] Q. Guo, M. Chen, Y. Liang, H. Chen, S. Yang, and S. Xie, "Photonics-assisted compressive sampling system for wideband spectrum sensing," *Chin. Opt. Lett.*, vol. 15, no. 1, 2017, Art. no. 010012, doi: 10.3788/COL201715.010012.

[12] Y. N. Kulchin, "Photonic sampled ADC's: State of the art," *Int. Soc. Opt. Photon.*, vol. 10176, Dec. 2016, Art. no. 1017618, doi: 10.1117/12.2268144.

[13] D. L. Donoho, "Compressed sensing," *IEEE Trans. Inf. Theory*, vol. 52, no. 4, pp. 1289–1306, Jan. 2006, doi: 10.1109/TIT.2006.871582.

[14] M. A. T. Figueiredo, R. D. Nowak, and S. J. Wright, "Gradient projection for sparse reconstruction: Application to compressed sensing and other inverse problems," *IEEE J. Sel. Topics Signal Process.*, vol. 1, no. 4, pp. 586–597, Dec. 2007, doi: 10.1109/JSTSP.2007.910281.

[15] V. K. Amalladinne, J. R. Ebert, J.-F. Chamberland, and K. R. Narayanan, "An enhanced decoding algorithm for coded compressed sensing with applications to unsourced random access," *Sensors*, vol. 22, no. 2, p. 676, Jan. 2022, doi: 10.3390/s22020676.

[16] J. F. C. Mota, N. Deligiannis, and M. R. D. Rodrigues, "Compressed sensing with prior information: Strategies, geometry, and bounds," *IEEE Trans. Inf. Theory*, vol. 63, no. 7, pp. 4472–4496, Jul. 2017, doi: 10.1109/TIT.2017.2695614.

[17] W. Lee, "Compressive sensing-based SAR image reconstruction from sparse radar sensor data acquisition in automotive FMCW radar system," *Sensors*, vol. 21, no. 21, p. 7283, Oct. 2021, doi: 10.3390/s21217283.

[18] G. Zhou, Y. Qi, Z. Heng Lim, and G. Zhou, "Single-pixel MEMS spectrometer based on compressive sensing," *IEEE Photon. Technol. Lett.*, vol. 32, no. 5, pp. 287–290, Jan. 31, 2020, doi: 10.1109/LPT.2020.2970742.

[19] J. M. Nichols and F. Bucholtz, "Beating Nyquist with light: A compressively sampled photonic link," *Opt. Exp.*, vol. 19, no. 8, pp. 7339–7348, 2011, doi: 10.1364/OE.19.007339.

[20] Y. Liang, M. Chen, R. Li, H. Chen, and S. Xie, "A photonic-assisted multi-channel compressive sampling system," presented at the IEEE Int. Topical Meeting Microw. Photon., Sep. 2012. [Online]. Available: https://ieeexplore.ieee.org/abstract/document/6474087

[21] Q. Guo, "Photonics-assisted compressive sampling system for wideband spectrum sensing," *Chin. Opt. Lett.*, vol. 15, no. 1, 2017, Art. no. 010012, doi: 10.3788/COL201715.010012.

[22] C. G. Valley, "Compressive sensing of sparse radio frequency signals using optical mixing," *Opt. Lett.*, vol. 37, no. 22, pp. 4675–4677, 2012, doi: 10.1364/OL.37.004675.

[23] B. Yang, H. Chi, S. Yang, Z. Cao, J. Ou, and Y. Zhai, "Broadband microwave spectrum sensing based on photonic RF channelization and compressive sampling," *IEEE Photon. J.*, vol. 12, no. 1, pp. 1–9, Feb. 2020, doi: 10.1109/JPHOT.2019.2960377.

[24] B. Yang, Q. Xu, S. Yang, and H. Chi, "Wideband sparse signal acquisition with ultrahigh sampling compression ratio based on continuous-time photonic time stretch and photonic compressive sampling," *Appl. Opt.*, vol. 61, no. 6, pp. 1344–1348, 2022, doi: 10.1364/AO.450386.

[25] S. Hong, H. Park, B. Shin, J.-S. No, and H. Chung, "A new performance measure using k-set correlation for compressed sensing matrices," *IEEE Signal Process. Lett.*, vol. 19, no. 3, pp. 143–146, Jan. 2012, doi: 10.1109/LSP.2012.2183365.
[26] S. Satpathi, R. L. Das, and M. Chakraborty, "Improving the bound on the RIP constant in generalized orthogonal matching pursuit," *IEEE Signal Process. Lett.*, vol. 20, no. 11, pp. 1074–1077, Nov. 2013, doi: 10.1109/LSP.2013.2279977.
[27] H. Ding, F. Lyu, H. Zhao, X. Niu, and C. Han, "Sub-Nyquist sampling method and its application in high-frequency electric-field measurement," *Opt. Eng.*, vol. 58, no. 11, Nov. 2019, Art. no. 114106, doi: 10.1117/1.OE.58.11.114106.
[28] J. A. Tropp and A. C. Gilbert, "Signal recovery from random measurements via orthogonal matching pursuit," *IEEE Trans. Inf. Theory*, vol. 53, no. 12, pp. 4655–4666, Dec. 2007, doi: 10.1109/TIT.2007.909108.
[29] M. A. Davenport and M. B. Wakin, "Analysis of orthogonal matching pursuit using the restricted isometry property," *IEEE Trans. Inf. Theory*, vol. 56, no. 9, pp. 4395–4401, Sep. 2010, doi: 10.1109/TIT.2010.2054653.
[30] D. Needell and R. Vershynin, "Uniform uncertainty principle and signal recovery via regularized orthogonal matching pursuit," *Found. Comput. Math.*, vol. 9, no. 3, pp. 317–334, Jun. 2009, doi: 10.1007/s10208-008-9031-3.
[31] D. L. Donoho, Y. Tsaig, l. Drori, and J.-L. Starck, "Sparse solution of under-determined systems of linear equations by stagewise orthogonal matching pursuit," *IEEE Trans. Inf. Theory*, vol. 58, no. 2, pp. 1094–1121, Feb. 2012, doi: 10.1109/TIT.2011.2173241.
[32] C.-B. Song, S.-T. Xia, and X.-J. Liu, "Improved analysis for subspace pursuit algorithm in terms of restricted isometry constant," *IEEE Signal Process. Lett.*, vol. 21, no. 11, pp. 1365–1369, Nov. 2014, doi: 10.1109/LSP.2014.2336733.
[33] M. S. Rao, K. K. Naik, and K. M. Reddy, "Radar signal recovery using compressive sampling matching pursuit algorithm," *Defence Sci. J.*, vol. 67, no. 1, p. 94, Dec. 2016, doi: 10.14429/dsj.67.9906.
[34] H. Yin, Y. Li, Y. Chai, Z. Liu, and Z. Zhu, "A novel sparse-representation-based multi-focus image fusion approach," *Neurocomputing*, vol. 216, pp. 216–229, Dec. 2016, doi: 10.1016/j.neucom.2016.07.039.
[35] J. Wen and H. Li, "Binary sparse signal recovery with binary matching pursuit," *Inverse Problems*, vol. 37, no. 6, Jun. 2021, Art. no. 065014, doi: 10.1088/1361-6420/abf903.
[36] X. Liao, S. Li, Y. Lu, and J. E. Roman, "A parallel structured Divide-and-Conquer algorithm for symmetric tridiagonal eigenvalue problems," *IEEE Trans. Parallel Distrib. Syst.*, vol. 32, no. 2, pp. 367–378, Feb. 2021, doi: 10.1109/TPDS.2020.3019471.
[37] S. Li, M. Gu, L. Cheng, X. Chi, and M. Sun, "An accelerated Divide-and-Conquer algorithm for the bidiagonal SVD problem," *SIAM J. Matrix Anal. Appl.*, vol. 35, no. 3, pp. 1038–1057, Jan. 2014, doi: 10.1137/130945995.

FANGXING LYU received the B.S., M.S., and Ph.D. degrees in measurement and instrumentation from Xi'an Jiaotong University, Xi'an, China, in 2007, 2010, and 2020, respectively. Since 2021, he has been a Lecturer at Xi'an Shiyou University. He is the author of two books, more than 20 articles, and six inventions. His current research interests include compressed sensing technology, optical fiber sensing technology, and photonics ADC technology.

FEI LI received the B.S. and M.S. degrees in measurement and instrumentation from Xi'an Jiaotong University, Xi'an, China, in 2000 and 2003, respectively, and the Ph.D. degree in electronic and electrical engineering from the University of Strathclyde, U.K., in 2006. Since 2018, he has been a Professor at Xi'an Shiyou University. He is also the Director of the Joint Laboratory of COSL and Xi'an Shiyou University. He is the author of three books, more than 30 articles, and 20 inventions. His current research interests include drilling automation technology, directional drilling technology, and high-speed ADC technology.

XIN FANG received the M.S. degree from the School of Computer Science, Shaanxi Normal University, Xi'an, China, in 2010. Since 2017, she has been an Associate Professor. She loves software design and very willing to share her software development experience with others. She is the author of three books, more than 20 articles, and three inventions. Her current research interests include software design and development, and computer education.

NAN ZHANG received the B.S. and M.S. degrees in measurement and instrumentation from Xi'an Shiyou University, Xi'an, China, in 2015 and 2018, respectively. Since 2018, he has been a Laboratory Master at Xi'an Shiyou University. He is good at circuit board design and debugging. His current research interests include measurement and control technology, and drilling automation technology. He led the students to win the first and second prizes of the national graduate electronic design competition many times.

XUEYING MA is currently pursuing the M.S. degree with Xi'an Shiyou University, China. She is good at Matlab simulation. Her current research interests include drilling automation technology and high-speed ADC technology.